ADVANCED HEALTHCARE MATERIALS
www.advhealthmat.de

Assessing Extracellular Vesicles in Human Biofluids Using Flow-Based Analyzers

*Kevin Ho Wai Yim, Olga Krzyzaniak, Ala'a Al Hrout, Ben Peacock, and Richard Chahwan**

Extracellular vesicles (EVs) are increasingly being analyzed by flow cytometry. Yet their minuscule size and low refractive index cause the scatter intensity of most EVs to fall below the detection limit of most flow cytometers. A new class of devices, known as spectral flow analyzers, are becoming standards in cell phenotyping studies, largely due to their unique capacity to detect a vast panel of markers with higher sensitivity for light scatter detection. Another class of devices, known as nano-analyzers, provides high-resolution detection of sub-micron-sized particles. Here, the EV phenotyping performance between the Aurora (Cytek) spectral cell analyzer and the NanoFCM (nFCM) nanoflow analyzer are compared. These two devices are specifically chosen given their lead in becoming gold standards in their respective fields. Immune cell-derived EVs remain poorly characterized despite their clinical potential. Therefore, B- and T-cell line-derived EVs and donor-matched human biofluid-derived EVs from plasma, urine, and saliva are used in combination with a panel of established immune markers for this comparative study. A comparative evaluation of both cytometry platforms is performed, discussing their potential and suitability for different applications. It is found that nFCM can accurately i) analyze small EVs (40—200 nm) matching the size accuracy of electron microscopy; ii) measure the concentration of a single EV particle per volume; iii) identify underrepresented EV marker subsets; and iv) provide co-localization of EV surface markers. It can also be shown that human sample biofluids have unique EV marker signatures that can have future clinical relevance. Finally, nFCM and Aurora have their unique strength, preferred fashion of data acquisition, and visualization to fit different research interests.

1. Introduction

Extracellular vesicles (EVs) are nano to micro-sized (40–1000 nm) lipid bilayer vesicles released by all cell types for intercellular communication. They achieve this through a plethora of signaling modalities including the transport of cargo molecules (nucleic acids, proteins, lipids, and other biomolecules) to recipient cells and surface receptor signaling.[1,2] They are found in all biological fluids and recent studies have shown their promising potential in disease diagnosis, prognosis, and therapeutics as well as vaccine development.[1,3–6] Recent emergence of fluorescence nanoparticle tracking analysis, microfluidic resistive pulse sensing (MRPS), fluorescence-based EV microscopy (Exoview), and single particle interferometric reflectance imaging (SP-IRIS) have accelerated the phenotyping of EVs. However, these platforms lack the quantitative power such as flow cytometric analysis for in-depth phenotyping capabilities in a high throughput manner.[7] Due to the small size and low refractive index of EVs, the scattering intensity is below the detection limit of common flow cytometers.[8,9] These hurdles have significantly slowed down the research progress in understanding the role of EVs in different life science research fields.

The active involvement of EVs in immune signaling and regulatory processes, ushers an urgent need for reliable and efficient turn-over analytics for immune EVs as quality assessment, as well as novel immune phenotyping tools.[1] Flow cytometry-based EV analyses mostly rely on antibody-bound bead-based capturing methods,[10,11] which help to overcome the size detection limit of conventional cytometers. Unfortunately, as no universally agreed upon EV marker is currently known,[12–14] this approach has the crucial drawback of overlooking all EV populations that do not express the specific capture marker of interest.[5] In addition, this type of analysis cannot provide single particle resolution since one bead can bind several EVs simultaneously and vice versa.

Label-free single particle nanoflow analyzers, first introduced by NanoFCM (nFCM) through the nanoflow analyzer, provide the rare opportunity of phenotyping EVs with the least pre-analytical filtering steps, with results proven by several studies in the past years.[3,15] Due to its two-laser conformation physical

K. H. W. Yim, O. Krzyzaniak, A. Al Hrout, R. Chahwan
Institute of Experimental Immunology
University of Zurich
Zurich 8057, Switzerland
E-mail: richard.chahwan@uzh.ch
B. Peacock
NanoFCM, ltd.
D6 Thane Rd, Nottingham NG90 6BH, UK

The ORCID identification number(s) for the author(s) of this article can be found under https://doi.org/10.1002/adhm.202301706

DOI: 10.1002/adhm.202301706

design, however, the number of fluorophore choices and their combinations are limited in the nFCM. Hence, we attempted to compare this system to a new class of flow cytometer, namely the Aurora (Cytek) spectral flow analyzer which utilizes photomultiplier tubes and a high number of detectors, allowing it to increase the number of resolvable fluorophores as well as its overall sensitivity for detection of particles above 100 nm in diameter given the precedence of usage of cells-based flow cytometer for EVs analyses.[16–20] Since immunological studies mostly focus on cell-to-cell interactions and signaling in the circulation of biofluids,[21–23] especially peripheral blood, we first benchmarked the two platforms using B- and T-cell line-derived EVs to verify the proposed antibodies panel and flow cytometers configuration.[24] The verified panel was further applied to analyze biofluid-derived EVs to reproduce the conditions of immunological and clinical studies through easily accessible liquid biopsies. We compared the size, concentration, and surface marker quantifications of sample EVs between the two platforms and ultimately described the beneficial properties of each platform for varying application goals. We also attempt to identify unique EV signatures in healthy biofluid donors to extrapolate clinical potentials.

2. Results and Discussion

2.1. Comparison of Quantification Sizing Capacities in Cell-Line Derived EVs

To compare the EV phenotyping capacity (size, concentration, and surface marker profile) between Aurora and nFCM, we began by benchmarking cell-line derived EVs, due to their i) size homogeneity, ii) controlled and reproducible yield from in vitro culture production, and iii) conserved parental cell marker expression for antibody panel benchmarking. Jurkat and Ramos cells were seeded in EV-depleted FCS media overnight at a cell density of 1 (10^7 cells mL^{-1}, after which EVs were harvested by serial centrifugation followed by flow analysis. The same sample sets were then sequentially measured on the two systems.

2.1.1. EV Size Comparison Among the Two Flow Devices

The size of both Jurkat and Ramos EVs was visualized using side scatter histograms (**Figure 1**A). Vesicle size distribution was estimated using reference beads from Apogee (default beads for Aurora analysis) and nFCM's four-peak beads (default beads for nFCM) with separate gates spanning the scatter signal peaks corresponding to each sizing bead population, in order to enhance the quantification power of sample vesicle size distribution (Figure S7A, Supporting Information). Using the Apogee beads, large EVs within 180–1300 nm in diameter, for which both cell lines seemed similarly enriched across all bins, could be identified by the Aurora (Figure 1B). The EV purification protocol however seemed particularly efficient for the isolation of small EVs (sEVs) as the vast majority of purified vesicles from both cell lines were found to be below 180 nm and even below 68 nm – the smallest detectable reference-bead population sizes of the Aurora and nFCM respectively (Figure 1A,B). In an aim to capture these smaller vesicles on the Aurora, and to test this platform's capacity for detection of vesicles down to 100 nm in diameter, nFCM sizing beads were acquired on the Aurora system. Of the four bead populations, only one peak was distinguishable from the background, this potentially being the 155 nm bead population (Figure S7B, Supporting Information). The peak largely overlapped with the 180 nm population of the Apogee beads, possibly in part due to the difference in refractive index between the two bead types (1.46 and 1.43 for the Apogee and nFCM beads respectively). We, therefore, determine that, in our hands, while the system may be able to detect smaller particles, background noise prevented the Aurora from resolving the particle size distribution of most vesicles by binning according to scatter peak signals of size reference beads below ≈155 to 180 nm in diameter. Consequently, the size of these smaller particles could only be assessed by the nFCM, where Jurkat EVs were slightly, but not significantly, more enriched in the 68 nm peak gate compared to Ramos EVs, while the latter was marginally more enriched in 91, 113, and 155 nm peak gates compared Jurkat EVs (Figure 1B).

2.1.2. EV Size Comparison in Relation with Transmission Election Microscopy

Using the nFCM size conversion algorithm based on the standard curve generated by sizing beads data, the overall mean size of sample EVs could also be determined (Figure 1C). These mean EV sizes were compared to transmission electron microscopy (TEM) data, which remains the de facto gold standard for accurate EV sizing (Figure 1D,E). With the aid of MAPS high-resolution image analysis software, the mean diameter of Jurkat and Ramos cell EVs was determined from just over 80 and 50 high-resolution TEM imaged EVs, respectively. Compared to size distribution interval data from nFCM, both Jurkat and Ramos cell EVs displayed very similar size distribution profiles, suggesting the sizing performance of nFCM is very comparable to that of the TEM. Furthermore, given the capacity of quantifying burst traces of sample particles in nFCM, thereby providing higher control in avoiding swarm effects, the nFCM software can produce direct particle concentration conversion using quality control (QC) beads of known concentration. Particle concentration yielded from the same number of EV-producing cells could therefore be quantified for the nFCM collected data (Figure 1F). This parameter also allowed us to assess the purity of our samples, where treatment with 0.1% Triton-X detergent showed a 79% and 80% mean concentration reduction in Jurkat and Ramos samples, respectively (Figure S1, Supporting Information). This was not possible in the case of the Aurora, where background noise and at least a 10% abort rate could not be avoided even after dilution and at the lowest flow rate.

2.2. Comparison of Fluorescence-Based Phenotyping Capacities in Cell-Line Derived EVs

Next, we compared the fluorescence detection performance of selected enriched EV markers, immune markers, and mem-

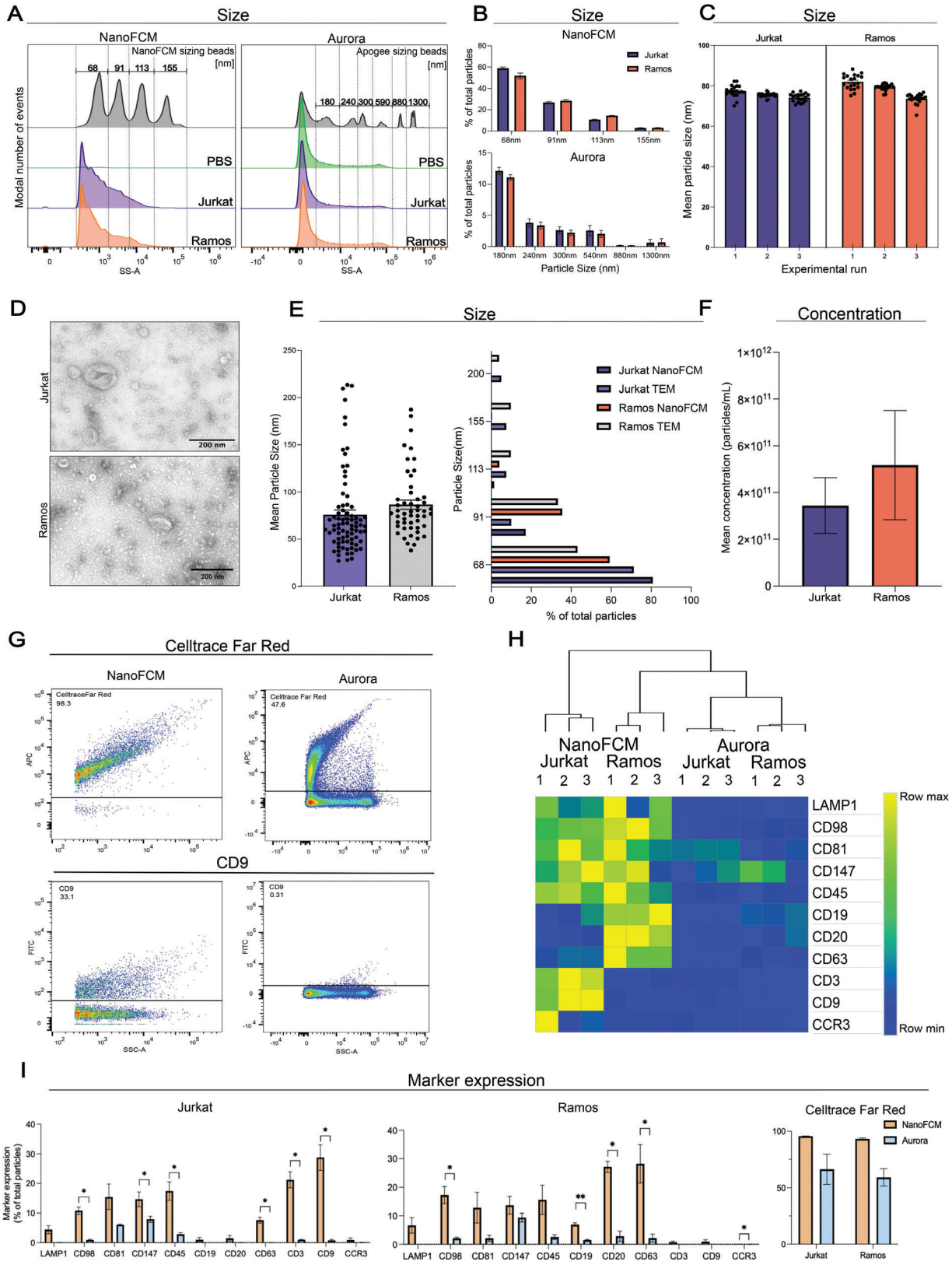

Figure 1. Jurkat and Ramos derived sEVs phenotyping using Cytek Aurora and NanoFCM nanoflow analyzer. A) Representative scatter histograms of comparison between the particle size distribution of Jurkat and Ramos derived sEVs with nFCM sizing beads (68, 91, 113, 155 nm) (left, nFCM) and Apogee sizing beads (right, Aurora), scatter area under modal peaks of sizing beads were used to gate for different particle size intervals. B) Approximated

brane dye of EVs from both cell lines using the two platforms (Figure 1G). Our antibody panel consisted of recently identified exosome-specific LAMP1, ectosome-specific CD147 (BSG) and CD98 (SLC3A2), plasma membrane dye (CellTrace Far Red), tetraspanins (CD9, CD63, and CD81), pan-leukocyte CD45, pan-B cell CD19 and CD20, pan-T cell CD3, and granulocytes specific CCR3 (Table S1, Supporting Information). Given the known discrepancies in machine flow rates between the nFCM and Aurora that might contribute to coincidence detection, also known as "swarm detection", serial dilutions of Jurkat EVs were performed to determine whether excess particles or unbound antibodies are affecting scatter or fluorescence signals. Stable fluorescence signal intensity of APC anti-CD45 was observed in both platforms while maintaining a linear relation between particle count and dilution factor (Figure S8, Supporting Information). To confirm CellTrace positive events are tetraspanins expressing EVs, co-expression of CellTrace Far Red, and CD81 in Jurkat and Ramos EVs. Over 93% of $CD81^+$ EVs from both cell lines were CellTrace positive, suggesting CellTrace staining covers the vast majority of EVs (Figure S9, Supporting Information). As expected, pan-B cell CD19 and CD20 mean expression were below 2% in Jurkat EVs, while pan-T cell CD3 mean expression was below 1% in Ramos EVs measured in both platforms, indicating the homogeneity of purified EVs and the specificities of antibodies (Figure 1H,I). CellTrace signals were predominantly over 90% in all samples measured with the nFCM platform, confirming the purity of EVs analyzed. CellTrace signal was strongly, though not significantly, reduced when the same samples were measured in parallel on the Aurora (Figure 1I). In Ramos EVs measured by nFCM, the top four most highly expressed markers were CD63, CD20, CD98, and CD147 at 28.3%, 27.2%, 17.3%, and 13.7% of total particles, respectively. This is relatively similar to results from Aurora, where the top four markers were CD147, CD20, CD45, and CD63 at 9.4%, 2.8%, 2.6%, and 2.2%, respectively. In Jurkat EVs measured by nFCM, the top four expressed markers were CD9, CD3, CD45, and CD81 at 29.0%, 21.2%, 17.4%, and 15.5% of total particles, respectively. Meanwhile, in Aurora, CD147, CD81, CD45, and CD3 were most highly expressed at 7.9%, 6.1%, 2.9%, and 1.02% of total particles, respectively. Overall, although the relative EV marker expression within the given panel is comparable between Aurora and NanoFCM in each source of EVs, the absolute percentages of such EV subsets were very different between the two platforms, for example, 21.2% versus 1.0% CD3 in Jurkat EVs and 27.2% versus 2.8% CD20 in Ramos EVs. This can possibly be due to differences in background noise level and/or EV particle size resolving window between the platforms, with nFCM covering EVs below 155 nm and Aurora above that size.

2.3. Comparison of Phenotyping Capacities in Three Human Biofluids Derived EVs

2.3.1. EV Sizing and Quantification Across the Three Human Biofluids

After establishing the fundamental parameters using cell-line EVs, we proceeded with the analysis of more complex biological samples. Plasma-, urine- and saliva-derived sEVs were used for phenotyping comparison due to their relevance in clinical studies and diagnostics. Size distributions of different biofluid-derived EVs were visualized using side scatter histograms (**Figure 2**A). Using size reference beads from Apogee (for Aurora analysis) and four peaks beads (for nFCM), we determined the majority of purified EVs in our samples to again be below 180 nm, as measured in the Aurora, and more specifically below 155 nm as measured in nFCM (Figure 2A,B). Scatter histograms from both Aurora and nFCM indicated larger vesicles were present in plasma compared to urine and saliva (Figure 2A). nFCM analysis was able to further resolve the differences in approximate size distribution between different sources of EVs, with saliva and urine EVs being more enriched than plasma in the 68 nm bin, while the latter was more enriched in bins of 91 nm and above (Figure 2B,C). Mean particle size data generated by the nFCM software reports also supported this result, showing plasma vesicles to be on average larger, with a mean particle size of 73.6 nm, than urine and saliva vesicles, which had mean particle sizes of 67.4 and 65.3 nm respectively. Interestingly, mean sEV concentration was found to be lowest in plasma with 1.5 (10^{10} particles mL^{-1}, followed by urine with 1.1 (10^{11} particles mL^{-1} and finally saliva with the highest concentration of EVs at 4.84 (10^{12} particles mL^{-1} (Figure 2D). This was quite unexpected due to the high complexity of blood and its role as a transport system connecting tissues all around the body.[26] This result could potentially be attributed to higher plasma EV aggregation and changes in morphology brought about by freeze–thawing or during ultracentrifugation, which are phenomena that have previously been reported in several studies, causing lower EV detection in these samples.[27,28] Purity of isolated EVs were also assessed by Celltrace Far Red staining (Figure 2E). Treatment with 0.1% Triton-X detergent, indicated high sample purity in all biofluids where mean concentration reduction in plasma, urine, and saliva was determined to be 84%, 85%, and 84% respectively (Figure S2, Supporting Information). PBS-HAT buffer was used as a storage buffer of stained EVs, however, higher buffer noise was observed in PBS-HAT compared to PBS only and no significant alterations in fluorescence signals or EV subset frequencies were observed (Figure S10, Supporting Information).

size distribution quantification of Jurkat and Ramos derived sEVs measured in nFCM and Aurora with particle size binning strategy in (A). C) Mean approximated particle size of sEVs in each nFCM experimental run as calculated by the nFCM analysis software in batches of two with three independent runs of each batch. D) Approximated size distribution and mean particle size quantification of Jurkat and Ramos derived sEVs TEM compared to nFCM analysis using particle size binning strategy in (A). E) Particle concentration quantification of Jurkat and Ramos derived sEVs measured in nFCM using standard QC beads with known concentration. F) Representative dot plots of CellTrace Far Red (R1 in Aurora; PC5 in NanoFCM) and CD9 (B2 in Aurora; B2 in NanoFCM) to demonstrate gating strategy. G) Clustered heatmap of denoted sEVs markers expression of Jurkat and Ramos's sEVs measured by nFCM and Aurora using Euclidean distance calculation. H) Quantification of sEVs markers of Jurkat and Ramos derived sEVs measured by nFCM and Aurora, values are representing the percentage of total measured particles. Multiple *T*-test, $p < 0.05$ *, $p < 0.01$ **, $p < 0.005$ ***, $n = 3$.

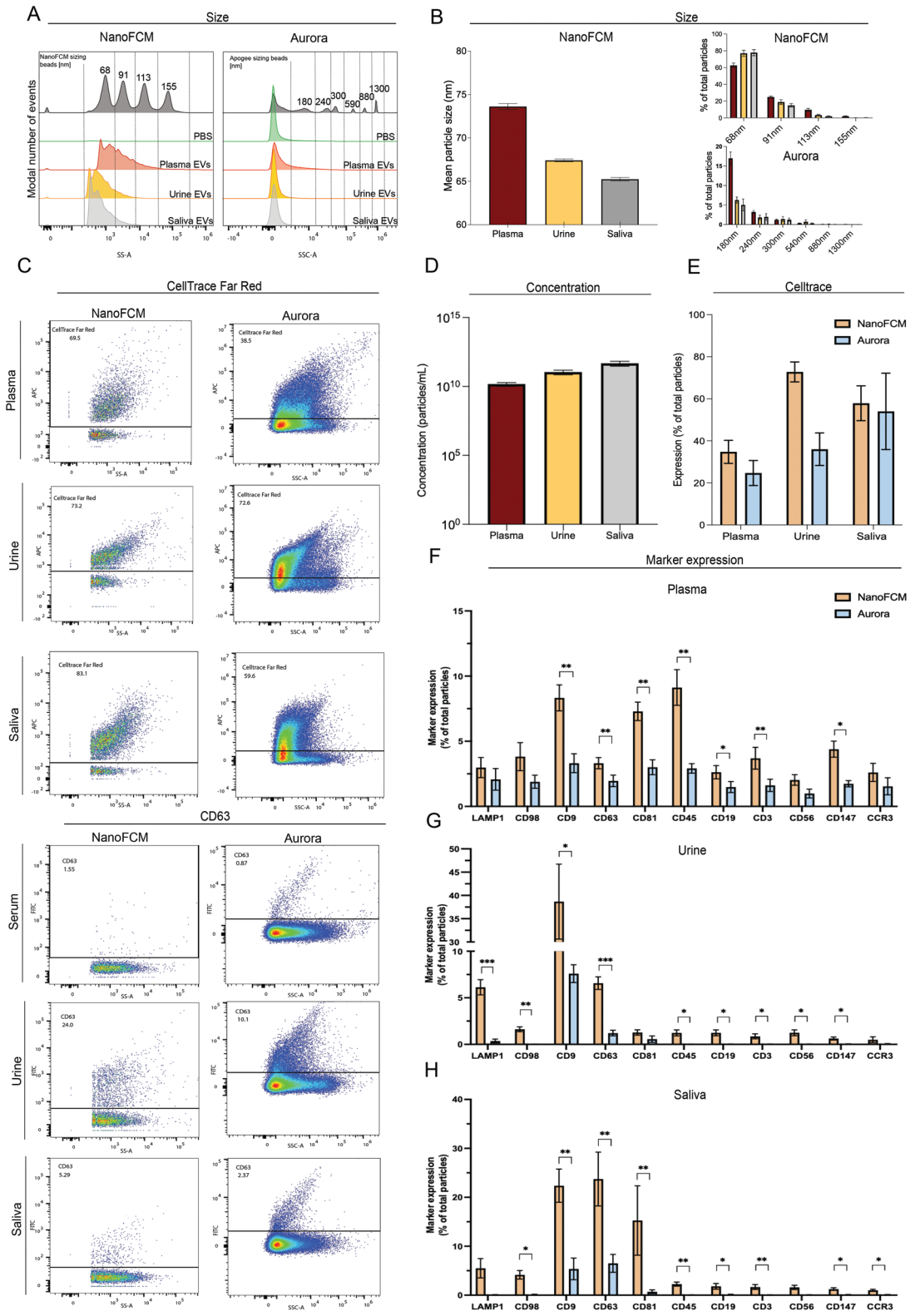

Figure 2. Healthy human donor biofluids derived sEVs phenotyping using Cytek Aurora and NanoFCM nanoflow analyzer. A) Representative scatter histograms of comparison between the particle size distribution plasma ($n = 6$), urine ($n = 6$), and saliva ($n = 4$) derived sEVs with nFCM sizing beads (68, 91, 113, 155 nm) (left, nFCM) and Apogee sizing beads (right, Aurora), scatter area under modal peaks of sizing beads were used to gate for different particle size intervals. B) Approximated binned size distribution quantification of cell-line EVs as measured by the nFCM and Aurora systems. C) Representative dot plots of CellTrace Far Red (R1 in Aurora; PC5 in nFCM) and CD63 (B2 in Aurora and nFCM) to demonstrate the gating strategy.

2.3.2. EV Surface Marker Detection Across the Three Human Biofluids

The fluorescence detection performance of selected enriched immune EV markers and membrane dye of biofluid-derived EVs was also compared between the two platforms (Figure 2C,F–H; Figure S3, Supporting Information). Isotype controls were performed to confirm the specificities of the antibodies (Figures S4,S5, Supporting Information). In plasma EVs, the top four markers detected in nFCM were CD45, CD9, CD81, and CD147 and similarly CD45, CD9, CD81, and CD63 in Aurora, which fits well with expectations for this type of biofluid. In urine EVs, CD9 was the most expressed marker measured in both platforms, however, CD66b, CD63, and LAMP1, which were detected in 7.6%, 6.6%, and 6.1% of particles by nFCM, could not be detected by Aurora. Similarly, in saliva sEVs, CD63 and CD9 were readily detected to different extents by both platforms, with CD63 expression being detected in 23.7% of particles in nFCM and 6.5% in Aurora and CD9 expression in 22.4% in nFCM and 5.4% in Aurora. The less expressed CD81 and CD66b could only be detected by nFCM however, where they were detected in 15.5% and 15.3% of vesicles respectively, and almost not at all in Aurora. In general, specialized immune cell markers, CD19, CD3, CD56, CD14, CD66b, and CCR3 were more enriched in plasma EVs compared to urine and saliva, Comparatively speaking, the two platforms showed comparable EV marker expressions within the given panel, however, the absolute percentages of markers between the two platforms were very different, 50% versus 10% CD9 in urine EVs for example, most likely due to differences in background noise level and particle size resolving window between the platforms. Moreover, lowly expressed markers were often below 1% positive in Aurora, making *de novo* EV markers identification from a percentage of total particles more challenging compared to nFCM. Comparison of particles per uL of analyzed EVs subsets as well as median fluorescence intensity of EVs subsets reduced the differences between the two platforms, suggesting both systems are comparable in detecting and quantifying fluorescent labeled vesicles (Figure S11, Supporting Information).

2.4. EVs Markers Can Define the Origin of Biofluids Irrespective of the Donor

Next, we attempted to define the origin of sEVs from different biofluids according to the distribution of our panel of selected markers. We performed principal component analysis (PCA) and dimension reduction correlation analysis of EV markers derived from different biofluids using the values from nFCM measurement due to its superiority in sEV markers detection seen in the above sections. Clear stratification of EV origin was observed, regardless of donor variabilities, from the unsupervised PCA Bi-plot exploratory analysis of four independent donor-derived plasma, urine, and saliva sEV markers (**Figure 3**A). Interestingly, CD3 (T-cell specific), CD45 (pan-leukocytes), and CD147 (plasma membrane protein) are the strongest drivers for the stratification between plasma and other EVs. Urine and saliva EV signatures were not as obvious as plasma EVs, with CD9 and LAMP1 (enriched in exosomes) being the strongest drivers for urine-derived EVs. CD66b (granulocyte specific) and CD63 were more represented in saliva EVs, while specialized immune EVs expressing CD14 (classical monocytes), CD19 (B-cell specific), CD56 (Natural Killer-cell specific), and CD98 (ectosomes enriched) markers were similarly represented in plasma and saliva EVs, that drove stratification from urine EVs. Spearman's correlation analysis of EV markers from different biofluid origins also revealed strong positive correlations between specialized immune EVs derived from plasma. Strong negative correlations were also observed between markers from plasma EVs and urine EVs (Figure 3B). Bi-plot and Spearman's correlation analysis in each type of biofluid measured in both Aurora and nFCM also revealed very different PC loadings and correlation patterns between our selected EV markers, suggesting the EVs landscape varied significantly in different biofluids (Figure S12, Supporting Information). These results further highlight the differential power of flow-based EV markers analysis in the identification of the origin of certain EV subsets, which is highly relevant in the diagnostic and prognostic application in clinical settings.

2.5. Comparative Evaluation of Aurora versus nFCM Flow Cytometers for EV Analysis

Depending on research aims and priorities, there are benefits and considerations to be weighed when deciding between the two platforms for EV studies. Our concluding results can be summarized as shown in **Table 1**. Since Aurora has been designed as a flow cytometer for cell phenotyping, it has a wider particle size window of sample analysis compared to nFCM which is specifically designed for sub-micron particles. The former platform would be useful if the samples were more heterogeneous, with sizes ranging up to a larger diameter, as the Aurora would provide higher flexibility in EV staining and efficiency in sample processing.[29] The inclusion of vesicles in the 200–1000 nm range in the sizing analysis by nFCM would require the use of an additional set of beads (not tested here) as well as additional measurements of the same samples with likely different dilutions. While possible, this would reduce the throughput of samples, which is already significantly lower than that of the Aurora. Overall, we find that Aurora requires less time and expertise for calibration, operation, and data analysis, which are important elements to be considered in mass-scale studies and high-throughput settings. However, this system is crucially limited by its inability to detect sEVs below ≈100 nm or, in our hands, to distinguish particles below ≈155 nm from the background. In protocols that are especially efficient for the isolation of sEVs,

D) Representative transmission electron microscopy images of Jurkat and Ramos cell-derived EVs. E) Particle concentration quantification of denoted biofluid-derived sEVs measured in nFCM using standard QC beads with known concentration. F) Quantification of CellTrace Far Red intensity in denoted biofluids derived sEVs measured by nFCM and Aurora for EVs purity assessment. G–I) Quantification of sEVs markers of plasma (G), saliva (H), and urine (I) derived sEVs measured by nFCM and Aurora, values are representing the percentage of total measured particles. $N = 6$. Multiple T-test, $p < 0.05$ *, $p < 0.01$ **, $p < 0.005$ ***.

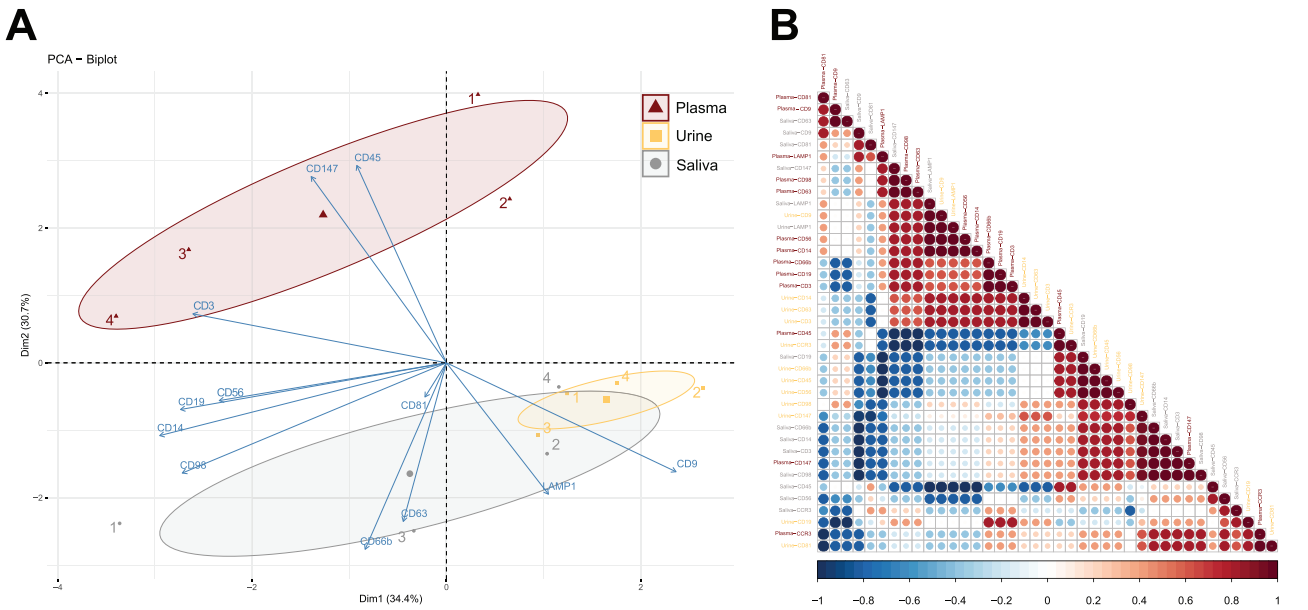

Figure 3. PCA and correlation of biofluids derived sEVs markers measured in NanoFCM nanoflow analyzer. A) PCA bi-plot analysis of EVs markers measured by NanoFCM stratifying different sources of biofluids EVs. Four individual human donors are indicated as 1, 2, 3, and 4. B) Spearman's rank correlation matrix of plasma, urine, and saliva sEVs markers from data acquired by NanoFCM. $N = 4$. One-way ANOVA, $p < 0.05$ *, $p < 0.01$ **, $p < 0.005$ ***.

this may cause issues as a large portion of EV events would be overlooked. The highly sensitive photon avalanche detectors allow the nFCM system to detect these smaller particles and therefore would be more beneficial if the samples are known to be sized under 200 nm. Other approaches like MRPS and SP-IRIS could be alternatives to validate sizes and EVs markers expression data generated by flow cytometric analysis as it has been shown certain aspects of the readout (sizes and concentrations) are comparable across the systems.[7]

It should also be noted that the particle size determined by both methods is only an estimation rather than a direct measurement of size. Slight inaccuracies in estimations may be unavoidable due to the possible discrepancies in the refractive index between EVs and silica-sizing beads. Since both methods rely on comparing the side scatter generated by silica beads to that of suspension EVs, it's critical for them to have refractive properties resembling each other as closely as possible. Though the small size of these vesicles does not permit sufficient space for diversity to cause major differences in the refractive properties of the EV population, variety will always exist and should be considered when interpreting this data.[30]

In terms of concentration quantification, the ability to quantify burst trace signals from scattering of each particle in nFCM provides a surplus advantage in phenotyping analysis as well as accurate EVs loading control for functional assays. In the context of surface marker profiling, nFCM is less affected by background noise possibly coming from photodiode detectors and sheath flow in the Aurora. Hence, EV fluorescence signals are

Table 1. Comparative table of benefits and considerations in Cytek Aurora and NanoFCM nanoflow analyzer for EVs analysis.

Parameters:	Cytek Aurora	NanoFCM
Resolvable particle size	>100 nm	40–200 nm
Particle concentration estimation	↓ (higher swarm effect)	↑ (Less swarm effect/Particle visualized as direct burst signals)
Side scatter detection of sEVs (<100 nm)	↓ (higher overlap with noise)	↑ (less overlap with noise)
Fluorescence detection of labeled sEVs (<100 nm)	↓ (Signals weaken by higher noise)	↑ (Less noise)
Fluorophore choices	↑ (5 lasers & up to 40 colors)	↓ (2 lasers & tighter emission bandwidth detection)
Ease of Operation & Throughput	↑ (Low expertise required set-up & <1 mi sample^{-1})	↓ (Expertise required set-up & ≈2 min sample^{-1})

less masked by the high background noise which is usually mixed within the negative EV population and ultimately leads to more accurate readout and increased sensitivity, especially in the case of detecting lowly expressed markers compared to the Aurora. Nevertheless, in the case of absolute particle count per volume in our sets of EV markers, discrepancies between the two platforms were reduced compared to the percentage of total particles, suggesting absolute particle count might be a more representative and accurate way to analyze EV subsets in Aurora by overcoming higher background noise. In terms of fluorophore choices, the Aurora is equipped with five lasers and can detect up to 40 different types of fluorophores on cells, while nFCM has only two lasers and a much tighter emission detection bandwidth. Provided the marker of interest is highly expressed and the samples are in the >100 nm size range, one could streamline their staining panel based on the flexible fluorophore options in Aurora, to simultaneously co-stain at least two or three markers of interest with the furthest emission wavelength from each to avoid spillover.

It is worth noting that the choice and combination of labeling dyes (>1 color/marker) are crucial parameters to avoid spillover of positive signals, throughout our study, we only co-labeled sample EVs with FITC (green) and APC (red) conjugated antibodies since the excitation/emission spectrum of the two fluorophores has the least overlap.[31] One could also consider using single-stained EV samples as well as antibody blocking to gauge the level of antibody competition in EV staining. Pre-processing steps of EVs from different types of liquid biopsy should also be carefully considered in EV flow analysis since their EV concentrations and purity are largely varied across sample types as well as donors. Thus, to ensure fair fluorescence quantification across samples, one can consider determining sample concentration and purity before antibody staining by particle counting and membrane dye analysis to better control the ratio of EVs and staining antibodies for more comparable and consistent results.

The swarming effect of the EVs is a further factor that should be taken into consideration when deciding between the two systems. While the Aurora does offer the option of lowering the flow rate, allowing us to reduce the swarming, this is not enough to alleviate the issue entirely. The abort rate throughout the samples was consistently high and diluting them only helped to resolve the issue marginally. Furthermore, we noticed some of the Auroras we tested were able to avoid swarming more efficiently than others, indicating that instrument setup can have a significant effect on the final experiment outcomes. NFCM on the other hand was able to reduce the swarming effectively, allowing us not only to retain a larger portion of the signal but also to effectively quantify the vesicles based on side scatter.

Finally, we found that nFCM data could be used to elucidate various marker correlation and association patterns through correlation mapping and PCA Bi-plot association analysis in biofluid EVs (Figure 3A,B). In plasma EVs especially, nFCM revealed far more complexity in marker correlations compared to Aurora where all markers were shown to positively correlate to various extents (Figure S12A,B, Supporting Information). Furthermore, we determined that nFCM biofluid data could be used to define clear stratification of biofluid sEV origin regardless of donor variabilities, through PCA Bi-plot analysis (Figure 3A). This could be particularly valuable when looking at patient samples, as changes in markers that are found to be associated with specific biofluids, or changes within the association patterns of those markers, could potentially be informative for diagnosis and monitoring of certain pathologies and therefore become highly relevant in clinical settings.

3. Conclusion

In conclusion, we evaluated the capabilities of two emerging technologies, the Aurora spectral cell analyzer and the NanoFCM nanoflow analyzer, in EV characterization and phenotyping. Both technologies exhibited distinct strengths and varied applications, particularly when exploring the complex realm of immune cell-derived EVs. The nFCM demonstrated notable proficiency in analyzing EVs ranging in size from 40 to 200 nm, confirming the concentration of individual EV particles per volume, pinpointing rare EV marker subsets, and facilitating the co-localization of EV surface markers. In contrast, Aurora was more adept at analyzing EVs larger than 200 nm and could detect EVs with multiple surface marker stains. The choice between these platforms is likely to depend on the specific research question and intended application, offering a comprehensive methodology for the in-depth study of EVs. Furthermore, our investigation uncovered unique EV marker signatures in human biofluid samples, such as plasma, urine, and saliva, suggesting promising avenues for clinical applications.

4. Experimental Section

Cell Cultures: Jurkat, a human T cell leukemia cell line, and Ramos, a Burkitt's lymphoma B-cell line, cells were maintained in Roswell Park Memorial Institute (RPMI-1640) medium (Sigma-Aldrich) supplemented with 10% Fetal Calf Plasma (Sigma Aldrich (non-American)), 1% Pen-Strep (Thermo Fischer), 1% Sodium Pyruvate 100 mM (Gibco), 5% NCTC-109 (Gibco), and 0.1% 2-Mercaptoethanol 50 mM (Gibco), at 37°C and 5% CO_2 and were split once 90% confluency was reached. Cells were cultured in EV-depleted FCS media at 1 (10^7 cells mL^{-1} in T175 (Sarstedt, #83.3912) overnight (18 h) before harvesting EVs. FCS EVs depletion was achieved by filtration using a 100 kDa ultrafiltration column (Merck, Cat.no. ACS510024) at 3000 g for 55 mins. Conditioned media was differentially centrifuged at 300 g to remove cells, 2000 g to remove debris, and 10 000 g to remove large particles and remaining debris, followed by centrifugation at 100 000 g (Sorvall Discovery 90SE ultracentrifuge) in a Fiberlite F50L-24 × 1.5 fixed-angle rotor (Thermo Fisher) for 1 h. All centrifugation steps were done at 4 °C. After this final purification step, the supernatant was removed using a vacuum pump, and pellets were resuspended in 0.22 µm filtered PBS at ≈8 (10^8 particles mL^{-1} in 50 uL aliquots stored in 4 °C in original UC tubes (Thermo Scientific, #15361379) prior to analyses and immunostaining within 1 h.

Biofluids Processing: Peripheral blood, urine, and saliva were drawn from three healthy male and three female volunteers between 20 and 50 years of age. For blood EVs, 3–5 mL of peripheral venous blood was collected into BD Vacutainer K2E (EDTA, 18 mg) 10 mL tubes (Beckton, Dickinson, and Co). After collection, peripheral blood was subjected to centrifugation at 2500 g for 10 mins at 4 °C for separation of plasma. Plasma was centrifuged at 10 000 g for 30 mins at 4 °C to remove large particles. Clarified plasma was split into 0.5 mL aliquots and stored at −80 °C until further use. In the case of saliva, 1 mL of the collected biofluid was diluted in 4 mL of 0.22 µm filtered PBS. Between 3 to 5 mL of undiluted urine and diluted saliva were centrifuged at 2000 g for 10 mins at 4 °C, and the remaining supernatants were centrifuged at 10 000 g for 30 mins at 4 °C to remove large particles. Clarified urine and saliva supernatant

were stored in 0.5 and 0.15 mL aliquots respectively and kept at −80 °C until further use.

On the day of the experiment, frozen biofluid EV aliquots were thawed quickly at 37 °C and distributed equally between ultracentrifugation tubes (Thermo Fisher) in preparation for ultracentrifugation. Samples were diluted 1:5 with 0.22 µm filtered PBS and were spun down at 100 000 g for 1 hour at 4 °C. Ultracentrifugation was found to produce EV samples of comparable purity to size exclusion chromatography in the previous publication.[3] After the final purification step, the supernatant was removed using a vacuum pump, and pellets were resuspended in 0.22 µm filtered PBS.

Immunostaining and Nanoflow Analysis of Purified EVs: Purified EVs were stained in 100 µL staining buffer with antibodies according to the defined panel (Table S1, Supporting Information) at 1:200 dilution in PBS and incubated for 30 mins at room temperature in the dark. Isotype control antibodies were used to test for unspecific binding, in addition to unstained EV suspension, PBS with antibodies only, and PBS-only procedural controls (Figures S1–S4, Supporting Information). To ensure no background signal was detected from any antibody aggregates or antibodies remaining after the final washing step, procedural controls with antibodies were prepared and measured alongside the panels. Following the incubation, selected samples (only FITC-antibody stained) were subsequently stained with 1 uL of CellTrace Far Red cell membrane dye (diluted in dimethyl sulfoxide (1:10 working solution)) (Thermo Fisher), and incubated in the dark for a further 30 min. The CellTrace dye was used for purity assessment, where a high percentage of positive events would indicate a low presence of non-vesicle contaminants. Stained EVs were washed with 1 mL of 0.22 µm filtered PBS at 100 000 g for 1 h to remove any remaining antibodies and potential antibody aggregates. Washed EVs were resuspended in 50 µl of 0.22 µm filtered PBS in 0.6 mL microtubes (Axygen, MCT-060-L-C) and subjected to flow analysis by NanoFCM Flow Nanoanalyzer (nFCM). PBS-HAT buffer, formulated according to[25] (HSA 0.2%; Trehalose 25 mM; HEPES 25 mM in PBS), was also used to resuspend washed EVs in one of the panels to test the potential enhancement in stability. Following this analysis, the samples were further diluted to minimize the abort rate due to swarming and analyzed with the Aurora. For purity assessment, Triton-X-100 detergent (PanReac AppliChem) was added to purified EVs at a final concentration of 0.1%, followed by vigorous vortexing for ≈30 s before acquisition. High purity would be indicated by a strong reduction in vesicle concentration and fluorescence after the treatment.

Purified EVs Analysis with nFCM: The instrument set-up was consistent across all experiments and followed recommendations from the manufacturer. Fluorescent 250 nm silica microsphere of known concentration (NanoFCM, QS2503, Lot 2 012 141, 2.07×10^{10} particles mL^{-1}) were used for QC and to quantify the particles detected in each sample. The beads were diluted at 1:100 and utilized to adjust measurement properties and laser power for optimization of sampling before each experimental run. For all experiments, the 525/40 and 670/30 filters were used for FITC detection using the 488 nm blue laser and for APC detection using the 640 nm red laser, respectively. Laser power was kept consistent for all runs, with 20 mW for the 488 nm laser and 40 mW for the 640 nm laser. The sampling pressure was adjusted to 0.8 kPa, and lasers were aligned as needed to achieve the highest possible peak intensity in the FITC, PC5, and SS-C channels. Threshold values were set using the auto function set to "small signal". Monodisperse silica nanoparticles (refractive index: 1.46) of four different sizes, with modal peak sizes of 68, 91, 113, and 155 nm were used as the size reference standard to calibrate the size distribution of EVs. Samples were recorded for 1 min within the range of 2000 to 12 000 events per minute. In cases where the concentration was too high, samples were diluted in filtered PBS accordingly. This allowed sufficient time/space distribution between the detected particles, minimizing the swarming as evidenced by the event burst trace indicating the separation of measured particles.

Purified EVs Analysis with Aurora: To compare the phenotyping capabilities of the Aurora and nFCM as closely and fairly as possible, the same set of samples was measured on both devices. Prior to the acquisition, the flow cell was soaked with Contrad for at least one hour with a 0.04 um inline sheath filter installed to minimize machine-associated noise. The threshold for side scatter was set to 800, and the gain of side scatter (SSC), B2 (FITC) and R1 (APC) detectors were set to 2500 with the aid of Apogee sizing beads (refractive index: 1.43) (#1527, Apogee Flow Systems), containing a mixture of sizing beads ranging from 80 to 1300 nm, of which, 110 and 500 nm beads population could be triggered by 488 nm laser to scatter green fluorescence for gating assistance from background noise. Briefly, threshold values were fine-tuned from the default value (50 000 SSC) until the entire sizing beads peaks could be resolved (Figure S6A,B, Supporting Information). Gain values were fine-tuned from default settings (200 SSC gain; 200 B2 gain; 200 R1 gain) until the 110 nm green fluorescence beads population could be clearly separated from the noise population (PBS blank control) along the SSC axis and B2 axis (Figure S6C, Supporting Information). PBS blank control was used to gate out background signal during fluorescence analysis, and sample acquisition was performed until the event rate of PBS was reduced to ≈1000 events per second (Figure S6C, Supporting Information). Unless stated otherwise, 80 000 events were recorded for all samples with the slowest flow rate (10 to 15 µl s^{-1}) to minimize the swarming effect.

Transmission Electron Microscopy of Purified EVs: EVs from 5 (10^6 cells were isolated and resuspended in 100 uL of 0.22 um filtered PBS. 50 uL of the EV suspension was used for analysis with the nFCM, while the remaining 50 uL was retained for TEM analysis. To visualize EVs samples under the TEM samples were transferred onto pioloform-coated EM copper grids by floating the grids on a droplet containing freshly prepared exosome placed on parafilm. After 5 min of incubation, the grids were washed 3 × 5 min on droplets of deionized water before contrasting bound exosomes in a mixture of 2% w/v methylcellulose and 2% w/v uranyl acetate (mix 9:1) on ice for 10 min. Contrasted grids were then air dried in a wire loop before analysis using a FEI Talos 120v. Images were taken with a digital CMOS camera BM-Ceta (Thermo Fisher). High-resolution images and particle size quantification analysis were acquired and performed by MAPS software (Thermo Fisher). TEM-measured vesicles within a specific diameter range were assigned to certain bead populations from the nFCM sizing beads (68, 91, 113, and 155 nm). The ranges were assigned as follows: 0–75 nm vesicles were assigned to the 68 nm peak, 76–98 nm to the 91 nm peak, 99–130 nm to the 113 nm peak, 131–180 nm to the 155 nm peak while all larger vesicles were assigned as being 200 nm.

Data and Statistical Analysis: EV flow cytometry data was exported as FCS files and analyzed using Flowjo software (Treestar). NFCM propriety software was used to generate FCS files and analytical reports with information regarding the sample concentration and mean particle size. Particle counts and volumetric data were obtained from Aurora experimental files (.EXPT) format for concentration per volume analyses. Statistical analysis of flow cytometry values was performed using GraphPad (version 9.1.1, GraphPad Software, La Jolla California USA) using multiple paired *t*-tests, where $*p < 0.05$, $**p < 0.01$, $***p < 0.001$. Hierarchical clustering in the heatmap was performed using one minus Pearson correlation through the Morpheus (Broad Institute) online software. High-resolution images and particle size quantification analysis were acquired and performed by MAPS software (Thermo Fisher). Spearman's correlation analyses were produced with RStudio software (version 4.0.1) using the "corrplot" package and implemented the "hclust" clustering method. PCA and Bi-plots were generated using the "factoextra", "ggfortify", and "ggplot2" packages.

Ethical Requirements: Human samples were covered by the Ethics Committee approval number 2019-00837

Supporting Information

Supporting Information is available from the Wiley Online Library or from the author.

Acknowledgements

K.H.W.Y. and O.K. contributed equally to this work. The authors thank Chahwan lab members for their comments; Joanne Lannigan (Cytek-Aurora) for insights and technical advice; and UZH flow cytometry and

microscopy facilities. R.C. was supported by SNSF (310030_212553; 320030E_215576, CRSK-3_190550; IZSEZ0_204655; IZSEZ0_218166), Novartis Foundation (22B140), Vontobel Stiftung (41309), UZH-STWF (F-41309-01-01), and the UZH-URPP (Translational Cancer Research). K.Y. was supported by a UZH BioMedTech Entrepreneur Fellowship and Bridge SNSF Proof of Concept (40B1-0_221565).

Open access funding provided by Universität Zurich.

Conflict of Interest

B.P. is employed at NanoFCM Co., Ltd. The remaining authors declare no conflict of interest.

Author Contributions

O.K., K.Y., and R.C. conceived the idea and coordinated the project. R.C. secured funding and guided the work. O.K. and K.Y. performed experiments and analyses. A.A. performed nFCM versus TEM sizing comparison. B.P. provided support on nFCM analysis and markers panel design. O.K. and K.Y. performed statistical data analyses. O.K. and K.Y. wrote the manuscript draft, which was edited by R.C.

Data Availability Statement

The data that support the findings of this study are available in the supplementary material of this article.

Keywords

biofluids, extracellular vesicles, liquid biopsies, nano-analyzers, nanoFCM

Received: May 29, 2023
Revised: August 2, 2023
Published online: October 25, 2023

[1] K. H. W. Yim, A.'a Al Hrout, S. Borgoni, R. Chahwan, *Cancers* **2020**, *12*, 3696.
[2] F. Cocozza, E. Grisard, L. Martin-Jaular, M. Mathieu, C. Théry, *Cell* **2020**, *182*, 262.
[3] K. Ho, W. Yim, S. Borgoni, R. Chahwan, *J. Extracell. Biol.* **2022**, *1*, e37.
[4] K. Dooley, R. E. Mcconnell, K. Xu, N. D. Lewis, S. Haupt, M. R. Youniss, S. Martin, C. L. Sia, C. Mccoy, R. J. Moniz, O. Burenkova, J. Sanchez-Salazar, S. C. Jang, B. Choi, R. A. Harrison, D. Houde, D. Burzyn, C. Leng, K. Kirwin, N. L. Ross, J. D. Finn, L. Gaidukov, K. D. Economides, S. Estes, J. E. Thornton, J. D. Kulman, S. Sathyanarayanan, D. E. Williams, *Mol. Ther.* **2021**, *29*, 1729.
[5] A. Hoshino, H. S. Kim, L. Bojmar, K. E. Gyan, M. Cioffi, J. Hernandez, C. P. Zambirinis, G. Rodrigues, H. Molina, S. Heissel, M. T. Mark, L. Steiner, A. Benito-Martin, S. Lucotti, A. D. Giannatale, K. Offer, M. Nakajima, C. Williams, L. Nogues, F. A. P. Vatter, A. Hashimoto, A. E. Davies, D. Freitas, C. M. Kenific, Y. Ararso, W. Buehring, P. Lauritzen, Y. Ogitani, K. Sugiura, N. Takahashi, *Cell* **2020**, *182*, 1044.
[6] L. Jiang, T. A. P. Driedonks, W. S. P. Jong, S. Dhakal, H. Bart van den Berg van Saparoea, I. Sitaras, R. Zhou, C. Caputo, K. Littlefield, M. Lowman, M. Chen, G. Lima, O. Gololobova, B. Smith, V. Mahairaki, M. R. Richardson, K. R. Mulka, A. R. Lane, S. L. Klein, A. Pekosz, C. Brayton, J. L. Mankowski, J. Luirink, J. S. Villano, K. W. Witwer, *J. Extracell. Vesicles* **2022**, *11*, e12192.
[7] T. Arab, E. R. Mallick, Y. Huang, L. Dong, Z. Liao, Z. Zhao, O. Gololobova, B. Smith, N. J. Haughey, K. J. Pienta, B. S. Slusher, P. M. Tarwater, J. P. Tosar, A. M. Zivkovic, W. N. Vreeland, M. E. Paulaitis, K. W. Witwer, *J. Extracell. Vesicles* **2021**, *10*, 12079.
[8] D. Lucchetti, A. Battaglia, C. Ricciardi-Tenore, F. Colella, L. Perelli, R. De Maria, G. Scambia, A. Sgambato, A. Fattorossi, *Int. J. Mol. Sci.* **2020**, *21*, 6257.
[9] U. Erdbrügger, J. Lannigan, *Cytometry, Part A* **2016**, *89*, 123.
[10] C. Campos-Silva, H. Suárez, R. Jara-Acevedo, E. Linares-Espinós, L. Martinez-Piñeiro, M. Yáñez-Mó, M. Valés-Gómez, *Sci. Rep.* **2019**, *9*, 2042.
[11] M.-N. Theodoraki, C.-S. Hong, V. S. Donnenberg, A. D. Donnenberg, T. L. Whiteside, *Cytometry, Part A* **2021**, *99*, 372.
[12] L. De Rond, E. Van Der Pol, C. M. Hau, Z. Varga, A. Sturk, T. G. Van Leeuwen, R. Nieuwland, F. A. W. Coumans, *Clin. Chem.* **2018**, *64*, 680.
[13] Z. Liao, L. M. Jaular, E. Soueidi, M. Jouve, D. C. Muth, T. H. Schøyen, T. Seale, N. J. Haughey, M. Ostrowski, C. Théry, K. W. Witwer, *J. Extracell. Vesicles* **2019**, *8*, 1628592.
[14] J. Kowal, G. Arras, M. Colombo, M. Jouve, J. P. Morath, B. Primdal-Bengtson, F. Dingli, D. Loew, M. Tkach, C. Théry, *Proc. Natl. Acad. Sci. U. S. A.* **2016**, *113*, E968.
[15] A. M. Silva, E. Lázaro-Ibáñez, A. Gunnarsson, A. Dhande, G. Daaboul, B. Peacock, X. Osteikoetxea, N. Salmond, K. P. Friis, O. Shatnyeva, N. Dekker, *J. Extracell. Vesicles* **2021**, *10*, e12130.
[16] J. A. Welsh, B. Killingsworth, J. Kepley, T. Traynor, K. Mckinnon, J. Savage, D. Appel, K. Aldape, K. Camphausen, J. A. Berzofsky, A. R. Ivanov, I. H. Ghiran, J. C. Jones, *Nanoscale* **2021**, *13*, 3737.
[17] A. L. Estrada, Z. J. Valenti, G. Hehn, A. J. Amorese, N. S. Williams, N. P. Balestrieri, C. Deighan, C. P. Allen, E. E. Spangenburg, N. A. Kruh-Garcia, D. S. Lark, *Am. J. Physiol., Cell Physiol.* **2022**, *322*, C246.
[18] G. I. Perez, D. Broadbent, A. A. Zarea, B. Dolgikh, M. P. Bernard, A. Withrow, A. McGill, V. Toomajian, L. K. Thampy, J. Harkema, J. R. Walker, T. A. Kirkland, M. H. Bachmann, J. Schmidt, M. Kanada, *Adv. Genet.* **2022**, *3*, 2100055.
[19] C. Coughlan, K. D. Bruce, O. Burgy, T. D. Boyd, C. R. Michel, J. E. Garcia-Perez, V. Adame, P. Anton, B. M. Bettcher, H. J. Chia, M. Konigshoff, E. W. Y. Hsieh, M. Graner, H. Potter, *Curr. Protoc. Cell Biol.* **2020**, *88*, e110.
[20] N. Z. Khan, T. Cao, J. He, R. M. Ritzel, Y. Li, R. J. Henry, C. Colson, B. A. Stoica, A. I. Faden, J. Wu, *Brain, Behav., Immun.* **2021**, *92*, 165.
[21] D. L. Bonilla, G. Reinin, E. Chua, *Front. Mol. Biosci.* **2020**, *7*, 612801.
[22] A. G. Spiteri, R. L. Terry, C. L. Wishart, T. M. Ashhurst, I. L. Campbell, M. J. Hofer, N. J. C. King, *J. Neuroinflammation* **2021**, *18*, 166.
[23] M. J. Camiolo, X. Zhou, T. B. Oriss, K. Nadeau, S. E. Wenzel, A. R. Correspondence, *Cell Rep.* **2021**, *35*, 108974.
[24] E. C. Sheppard, R. B. Morrish, M. J. Dillon, R. Leyland, R. Chahwan, *Front. Immunol.* **2018**, *9*, 0355.
[25] A. Görgens, G. Corso, D. W. Hagey, R. Jawad Wiklander, M. O. Gustafsson, U. Felldin, Y. Lee, R. B. Bostancioglu, H. Sork, X. Liang, W. Zheng, D. K. Mohammad, S. I. Van De Wakker, P. Vader, A. M. Zickler, D. R. Mamand, L. Ma, M. N. Holme, M. M. Stevens, O. P. B. Wiklander, S. El Andaloussi, *J. Extracell. Vesicles* **2022**, *11*, e12238.
[26] J. He, W. Ren, W. Wang, W. Han, L. Jiang, D. Zhang, M. Guo, *Drug Delivery Transl. Res.* **2022**, *12*, 2385.
[27] J. Machhi, F. Shahjin, S. Das, M. Patel, M. M. Abdelmoaty, J. D. Cohen, P. A. Singh, A. Baldi, N. Bajwa, R. Kumar, L. K. Vora, T. A. Patel, M. D. Oleynikov, D. Soni, P. Yeapuri, I. Mukadam, R. Chakraborty, C. G. Saksena, J. Herskovitz, M. Hasan, D. Oupicky, S. Das, R. F. Donnelly, K. S. Hettie, L. Chang, H. E. Gendelman, B. D. Kevadiya, *J. Neuroimmune Pharmacol.* **2021**, *16*, 270.
[28] R. Linares, S. Tan, C. Gounou, N. Arraud, A. R. Brisson, *J. Extracell. Vesicles* **2015**, *4*, 29509
[29] Cytek Aurora Say Hello to a New Reality, https://welcome.cytekbio.com/hubfs/Website%20Downloadable%20Content/Brochures/N9-20001_cytek_aurora_brochure.pdf.
[30] C. Gardiner, M. Shaw, P. Hole, J. Smith, D. Tannetta, C. W. Redman, I. L. Sargent, *J. Extracell. Vesicles* **2014**, *3*, 25361.
[31] D. Fortunato, D. Mladenović, M. Criscuoli, F. Loria, K. L. Veiman, D. Zocco, K. Koort, N. Zarovni, *Int. J. Mol. Sci.* **2021**, *22*, 10510.